Measurement 197 (2022) 111295

Contents lists available at ScienceDirect

Measurement

journal homepage: www.elsevier.com/locate/measurement

# A practical and general methodology for efficiency calibration of coaxial Ge detectors

A. Barba-Lobo *, J.P. Bolívar

*Department of Integrated Sciences, Center for Natural Resources, Health and Environment (RENSMA), University of Huelva, 21071 Huelva, Spain*

ARTICLE INFO

*Keywords:*
Gamma-ray spectrometry
Efficiency calibration
Artificial and natural radionuclides
True coincidence summing
Self-absorption
Dead time

ABSTRACT

The correct determination of artificial and natural radionuclides like $^{152}$Eu, $^{137,\ 134}$Cs, $^{60,\ 57}$Co, etc., and $^{234,\ 228}$Th, $^{228,\ 226}$Ra, $^{210}$Pb and $^{40}$K, respectively, is essential for many environmental science fields. For this, a general function was obtained for the full-energy peak efficiency (*FEPE*) by gamma-ray spectrometry using coaxial Ge detectors. Then, the experimental *FEPE* values, obtained fixing the energy, $E_\gamma$, were fitted varying the thickness, $h$, of cylindrical standards. The parameters resulted from these fittings were fitted, in turn, versus $E_\gamma$, obtaining a general efficiency function, $\varepsilon_c\ (E_\gamma, h)$. $\varepsilon_c\ (E_\gamma, h)$ was validated, obtaining very good $z_{score}$, except for $E_\gamma$ affected by TCS effects. Consequently, a practical and general method was developed, recalibrating the detector by varying the sample-detector distance, $d$. $\varepsilon_c\ (E_\gamma, h, d)$ was obtained, achieving very good $z_{score}$. Furthermore, this practical method was also employed to correct high self-absorptions and high dead times.

## 1. Introduction

There are several natural and artificial radionuclides of interest within the field of the environmental radioactivity, such as $^{234,\ 228}$Th, $^{228,\ 226}$Ra, $^{210}$Pb and $^{40}$K, as well as $^{241}$Am, $^{152}$Eu, $^{137,\ 134}$Cs, $^{133}$Ba, $^{60,\ 57}$Co. In order to determine these radionuclides by gamma-ray spectrometry, it is of vital importance to use different types of detector efficiency corrections. Among the most important efficiency corrections, there are the following: true coincidence summing (TCS), self-absorption and dead time corrections.

Regarding the former correction type, they are often applied to determine artificial radionuclides, given that the majority of artificial radionuclides have TCS effects ($^{152}$Eu, $^{137,\ 134}$Cs, $^{60,\ 57}$Co, etc.). However, some natural radionuclides like $^{214}$Bi and $^{208}$Tl, which are daughters of $^{226}$Ra and $^{228}$Th corresponding to the $^{238}$U- and $^{232}$Th-series, respectively, also suffer TCS effects [1–3]. Therefore, this type of correction is indispensable to be considered in order to know the radionuclide activity concentrations in a proper way. Furthermore, it is necessary to clarify that there are two kinds of TCS effects: “summing in” and “summing out” effects. The former takes place when two photons are detected simultaneously and they are added to a specific full-energy peak, where those two photons have energies that do not belong to that specific peak. The second type consists in the opposite phenomenon, that is, one of those two simultaneous photons is taken away from that specific peak and included in another peak.

In the case of the TCS corrections, nowadays the corrections provided by MCNP, GEANT4, PENELOPE or FLUKA simulation codes have become generalized [4–11]. However, in order to carry out these corrections by using simulation software, it is necessary to characterize the detector parameters and, consequently, expensive costs and several months are required, being the detector inoperative during the time taken to carry out the detector characterization procedure.

With respect to the self-absorption corrections, they are very useful to be employed due to the possible chemical composition and density differences between the samples used to calibrate the detectors and the other samples, which are called as problem samples. The reason is because when the composition and density of the calibration and problem samples are very different from each other, the photons are attenuated differently and, consequently, a self-absorption correction is required to introduce these differences in the detector efficiency calculation when this is obtained in the problem sample matrices [12–14]. Besides that, self-absorption corrections are essential in the cases of the radionuclides whose gamma emissions belong to the low energy range, that is, energies less than 150 keV, since the self-absorption effects are much more relevant for that energy range [15–17].

On the other hand, regarding the dead time corrections, they are usually employed in the cases for which samples, whose radionuclides have very high activity concentrations, are measured. In these cases,

* Corresponding author.
*E-mail address:* alejandro.barba@dci.uhu.es (A. Barba-Lobo).

https://doi.org/10.1016/j.measurement.2022.111295
Received 28 December 2021; Received in revised form 3 April 2022; Accepted 30 April 2022
Available online 6 May 2022

given that there is a large number of disintegrations per second, the detector is not able to detect all photons that reach the detector. Consequently, a great number of events are not considered and, therefore, not included in the activity concentration calculations, determining the radionuclides in an improper way.

For all reasons previously mentioned, this study aims to develop a new and simple methodology to correct TCS and self-absorption effects, as well as high dead times. For this, a recalibration of the detector was accomplished, obtaining a general efficiency function in the calibration matrix, $\varepsilon_c$ ($E_\gamma$, $h$, $d$), based on the full-energy peak efficiency (*FEPE*), and which depends on the gamma emission energy ($E_\gamma$), the sample thickness ($h$) and the distance ($d$) existing between the bottom of the selected geometry (cylindrical in our case) and the detector window.

## 2. Materials and methods

### 2.1. Materials

In order to carry out this study, an extended range high purity germanium detector (XtRa) was employed. The XtRa detector has a relative efficiency of 38.4% in relation to a 3″ × 3″ NaI (Tl) detector, a full width at half maximum (FWHM) of 1.74 keV and 0.88 keV at 1332 keV and 122 keV, respectively, and a peak-Compton relation of 67.5:1. The XtRa detector is connected to a FET preamplifier whose model is 2002 CSL, where the bias voltage value used for this detector was 3500 V. In order to proceed with the cooling of this detector, $LN_2$ was employed for it.

On the other hand, to accomplish the corrections related to TCS effects and high dead times, a simple and general mechanism was designed, which consists in a cylindrical polyvinyl chloride (PVC) tube that was pierced from two opposite sides. Therefore, trough the holes made on the surface of the hollow tube, it is possible to introduce screws that are thick and long enough to properly hold the sample support, allowing us to place the samples at a distance from the detector window (see Fig. 1). As can be seen in Fig. 1, the PVC tube was attached to a base, which is also composed of PVC, making the tube more stable. Regarding the holes made on the tube surface, it is necessary to clarify that the first hole is placed at 25 mm of height from the detector window and the second one is 10 mm above the first one, being this height the same one between two consecutive holes.

Regarding the samples selected to accomplish this work, certified standards provided by the IAEA (International Atomic Energy Agency) were employed to proceed with the detector calibration, whose codes and reference activity concentrations are RGU-1, RGTh-1 and RGK-1, and 4940(15) Bq $kg^{-1}$ 3250(45) Bq $kg^{-1}$ and 14000(200) Bq $kg^{-1}$, respectively. These calibration standards contain radionuclides belonging to the $^{238}$U- and $^{232}$Th-series, as well as $^{40}$K, respectively, being all radionuclides in secular equilibrium in the two series. For further information about RGU-1, RGTh-1 and RGK-1 standards, see [18,19]. Then, several problem NORM (Naturally Occurring Radioactive Materials) samples were also chosen which are characterized by having a very wide variety of chemical compositions and densities, allowing us to do a much more complete study. These problem samples can be classified into two groups: samples whose activity concentrations are known and not known. See [20–23] for further information about NORM samples.

With respect to the former type, they are the following: a soil sample (Soil-1), a milk powder sample (Milk powder), two water and furnace slag samples (Furnace slag, Water-1 and Water-5), as well as another soil sample (Soil-2), that were employed in the Inter-comparison – CSN/CIEMAT exercises carried out in 2016, 2018, 2019 and 2020, respectively. In addition, samples used in the Inter-comparison – IARMA exercise carried out in 2020 were selected, which were a seaweed sample (IARMA-097) and three water samples (IARMA-098, IARMA-099 and IARMA-100). Besides that, three soil samples provided by the IAEA were chosen (IAEA-326, IAEA-327 and IAEA-375), as well as a potassium carbonate sample ($K_2CO_3$) and a tin concentrate sample (Sn-Sample). Regarding CSN, CIEMAT and IARMA, they are the acronyms for the Spanish Nuclear Safety Council (“Consejo de Seguridad Nuclear”), the Centre for Energy, Environment and Technology Research (“Centro de Investigaciones Energéticas, Medioambientales y Tecnológicas”) and the International Atomic Reference Material Agency, respectively.

Then, regarding the latter sample kind (samples whose activity concentrations are not known), the following samples were selected: three industrial wastes known as scales (Scale-A, Scale-B and Scale-C). See Table A.11 in Supplementary Material for further information about all samples chosen in this study. Furthermore, it is necessary to clarify that in this study, there is not any sample whose radioactive index is higher than the thresholds defined for radioactive facilities.

### 2.2. Methods

In order to obtain the $\varepsilon_c$ ($E_\gamma$, $h$) function, that is, the efficiency function without incorporating TCS corrections, the results obtained in a previous work [24] was used. In [24], a methodology to calibrate in efficiency varying the sample thickness was developed without studying any correction type in depth. However, in the present study, TCS and self-absorption effects, as well as high dead-times were studied in depth, developing an exhaustive methodology in order to correct them. To proceed with the obtaining of $\varepsilon_c$ ($E_\gamma$, $h$), the calibration standards were compacted until reaching the desired thickness values ($h$), where $h$ values were ranged from 5 mm to 45 mm in the case of RGU-1 standard, from 5 mm to 50 mm in the cases of the RGTh-1 and RGK-1 standards. For the three standards, an apparent density about 1.63(2) g $cm^{-3}$ was measured. Then, the experimental values of the full-energy peak efficiency (*FEPE*) were calculated for the different selected $h$ and $E_\gamma$ values. Finally, a function was chosen to fit the experimental *FEPEs* varying $h$ and fixing $E_\gamma$, $\varepsilon_c(h)$.

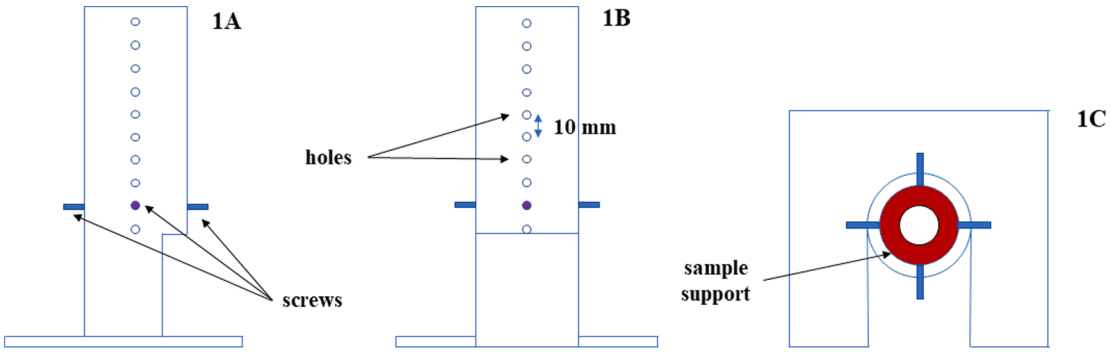


**Fig. 1.** Several perspectives of the system employed, a PVC tube, in order to proceed with the efficiency corrections: 1A) Profile; 1B) Side used to fit the PVC tube with the detector; 1C) Top.

Once the experimental *FEPE* values were fitted by $\varepsilon_c(h)$, varying $h$ and fixing $E_\gamma$, the parameters resulted from these fits, $pr_i(E_\gamma)$, were also fitted versus $E_\gamma$. It is necessary to clarify that in order to carry out the fits for $pr_i(E_\gamma)$, only high energies were selected, that is, $E_\gamma > 150$ keV (see Table A.3 in Supplementary Material for further information about the $E_\gamma$ chosen in this study). Let us call this efficiency function as $\varepsilon_c(E_\gamma > 150$ keV, $h)$. The reason why only $E_\gamma$ values belonging to the high energy range were selected was because there were only a few $E_\gamma$ values of interest less than 150 keV. Therefore, a general efficiency function was obtained for any $h$ and $E_\gamma$ values found between 5 mm and 50 mm, and 186 keV and 1765 keV, respectively. After determining the general $\varepsilon_c(E_\gamma > 150$ keV, $h)$ function, it was necessary to introduce the self-absorption corrections, in order to calculate the detector efficiency in any problem sample matrix. Note that this general function, which has been obtained by using calibration standards that contain only natural radionuclides, can also be employed to determine artificial radionuclides.

On the other hand, to introduce the TCS corrections in the obtained efficiency function, a PVC tube was employed which was previously described. Several values of the distance between the geometry bottom and the detector window, $d$, were chosen: 0, 25, 35, 45, 55 and 65 mm. In this case, to carry out the detector calibration in efficiency, only the RGU-1 standard was used. This standard was prepared for a fixed $h$ value of 25 mm, and it was measured for each one of the $d$ values mentioned.

Then, there are several methods to determine and correct the dead time, among which is the method called as the two sources method. This method consists of comparing the counting rates obtained from two individual point sources and the ones obtained in a combination of the two sources [25–28]. An alternative method, which does not need for any source combinations or tedious procedures, as well as it has not been studied in previous works, will be employed in this study in order to correct the dead time. The method proposed in this study for the high dead time corrections (see Section 3.5) is analogous to the one previously described for TCS corrections. The dead time depends on the resolution time of the Ge detector and on the electronics (preamplifier, amplifier, Analog-to-Digital Converter (ADC), etc.). Therefore, the dead time has a strong dependence on the total efficiency and the sample activity for a specific detection system. In applications involving a high rate of incoming radiation, detection systems can lose a significant amount of data. Consequently, increasing the source-detector distance, the particle rate that reach the detector is reduced and, therefore, the dead time of the system will be reduced, being our methodology to correct the dead time based on this idea. In this case, the same $d$ values were also selected to carry out the dead time corrections (0, 25, 35, 45, 55 and 65 mm).

## 3. Results and discussion

### 3.1. Obtaining of the $\varepsilon_c(E_\gamma > 150$ keV, $h)$ function

Firstly, it is necessary to define the equation used to calculate the experimental *FEPE* values, given that they are required in order to obtain the $\varepsilon_c(E_\gamma, h)$ function:

$$\varepsilon_c^{exp} = \frac{G - B - F - I}{P_\gamma \; a \; m_c \; t} \tag{1}$$

where $G$, $B$, $F$, and $I$ are the total number (gross) of counts for the photopeak of interest whose gamma emission energy is $E_\gamma$, the Compton continuum, the background and the interference term, respectively. Then, each $E_\gamma$ is characterized by having a probability of gamma emission, $P_\gamma$, which were taken from [29]. On the other hand, $a$ and $m_c$ are the activity concentration and mass of the standard, respectively, used in the calibration procedure, being $t$ the measurement time.

Regarding the $P_\gamma$ value obtained for 186 keV ($^{226}$Ra), secular equilibrium between $^{238}$U and $^{226}$Ra was considered. Let us call the emission probability resulted from this case as $P_\gamma^*$, where $P_\gamma^* = P_\gamma(^{226}\text{Ra}) + {}^{235}\text{U}/^{238}\text{U}\; P_\gamma(^{235}\text{U}) = 6.14(6)\%$, being $P_\gamma(^{226}\text{Ra}) = 3.51(6)\%$ and $P_\gamma(^{235}\text{U}) = 57.2(5)$ % at 186 keV, and $^{235}\text{U}/^{238}\text{U} = 0.046$ [30]. Besides, the emission probability value related to this case, as well as the ones corresponding to the other energies selected for natural radionuclides have been shown in Table A.3.

Once the experimental *FEPEs* have been calculated, they can be fitted by a semi-empirical function. In our case, it has been checked that the function which provides the best fits for the experimental *FEPEs* is the one given by the following equation:

$$\varepsilon_c(h) = pr_1 exp(pr_2 h) + pr_3 \tag{2}$$

where $pr_i$ (with i = 1, 2, 3) are parameters resulted from the fits of the experimental *FEPEs* versus $h$ (standard thickness) for each $E_\gamma$ (gamma emission energy) value, being possible to find the $pr_i$ values resulted from the fits at each $E_\gamma$ value in Tables A.1 and A.2 (see Supplementary Material). See [24] for further information about the obtained experimental *FEPEs* and the fits carried out for them.

After obtaining the $pr_i$ values, they have been plotted versus $E_\gamma$ (see Fig. 2). Furthermore, in Fig. 2 it is also possible to see the fits carried out for $pr_i$ versus $E_\gamma$. It is easy to realize that $pr_i$ values can be fitted by using a lineal function, which can be written by the following equation:

$$ln(|pr_i(E\gamma)|) = pr_{i1} + pr_{i2}\, ln(E_\gamma/E_0) \tag{3}$$

where $pr_{ij}$ (with j = 1, 2) are the parameters resulted from the fits and $E_0$ = 1 keV.

Besides, the $pr_{ij}$ parameter values have been shown in Fig. 2, as well as the relative average residuals, <Residual> (%), and $R^2$ values resulted from these fits, where the obtained <Residual> and $R^2$ values were 3.7%, 4.6% and 4.1%, and 0.994, 0.91 and 0.990 for $pr_1$, $pr_2$ and $pr_3$, respectively. Therefore, the fitting functions agreed very well with the $pr_i$ values.

If $pr_i(E_\gamma)$ function given by Eq. (3) is inserted in Eq. (2) for each i value, it is possible to rewrite Eq. (2) in the following way:

$$\begin{aligned}\varepsilon_c(E_\gamma, h) = {} & exp\left[pr_{11} + pr_{12}\ln\left(E_\gamma/E_0\right)\right] exp\left(exp\left[pr_{21} + pr_{22}\ln\left(E_\gamma/E_0\right)\right] h\right) \\ & + exp\left[pr_{31} + pr_{32}\ln\left(E_\gamma/E_0\right)\right]\end{aligned} \tag{4}$$

where $\varepsilon_c(E_\gamma, h)$ is the general efficiency function obtained varying the gamma emission energy, which can be called as $\varepsilon_c(E_\gamma > 150$ keV, $h)$ if only high $E_\gamma$ values are taken.

On the other hand, it is necessary to clarify that not all gamma energies selected in the detector calibration were employed to carry out the $pr_i$ fits. In Table A.3, a specification was made on which $E_\gamma$ values were chosen in order to fit $pr_i$. Furthermore, in Table A.3, it is interesting to observe that the majority of the $E_\gamma$ values that have been discarded to fit $pr_i$, having checked that they were outliers, are gamma energies belonging to $^{214}$Bi (such as 609 keV, 768 keV, 1120 keV and 1238 keV) and $^{208}$Tl (583 keV). The data considered as outliers were those for which $\left(y_{exp} - y_{fit}\right) \Big/ \sigma_{exp} > 3$, where $y_{exp}$, $\sigma_{exp}$ and $y_{fit}$ are the experimental value and its uncertainty at 2 sigma level, and the value provided by the fitting function, respectively. Note that they are energies clearly affected by TCS effects, and this will be demonstrated in this Section and in Section 3.2. Consequently, the $pr_i$ values corresponding to those energies do not usually follow the same behaviour than the ones obtained for the other energies, this occurring more clearly for $pr_1$ since this parameter is characterized by having more dependence on $E_\gamma$, while this dependence is much less significant in the $pr_2$ case.

Once the $\varepsilon_c(E_\gamma > 150$ keV, $h)$ function has been obtained, applications of $\varepsilon_c(E_\gamma > 150$ keV, $h)$ to problem samples, as well as validations of this function have been carried out. For this, it is necessary to transform it to the detector efficiency obtained in any problem sample matrix. For this, it is required to apply the self-absorption correction factor given by the Cutshall's model [31,32]:

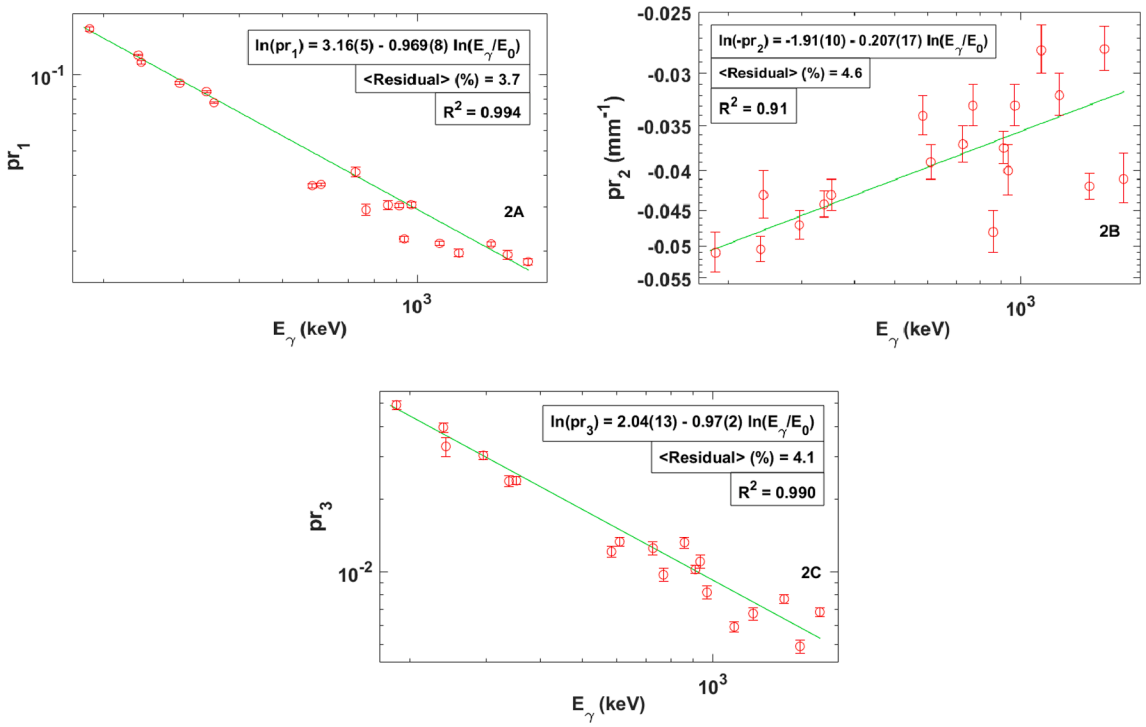


**Fig. 2.** Fits carried out for the $pr_i$ parameters in order to obtain the general efficiency function at high energies, $\varepsilon_c(E_\gamma > 150\ \text{keV}, h)$: 2A) $pr_1$; 2B) $pr_2$; 2C) $pr_3$. Furthermore, relative average residuals and $R^2$ values have been calculated for each fit of $ln(pr_i)$ versus $ln(E_\gamma/E_0)$.

$$f_a^C(E_\gamma, h, \eta, \eta_c, \rho, \rho_c) = \frac{\eta_c \rho_c (1 - exp(-\eta\rho h))}{\eta\rho (1 - exp(-\eta_c \rho_c h))} \quad (5)$$

where $h$ and $E_\gamma$ are the problem sample thickness and the energy for which the self-absorption correction is being applied, respectively, $\rho$ and $\rho_c$ are the apparent densities corresponding to the problem and calibration samples, respectively. Then, $\eta$ and $\eta_c$ are the mass attenuation coefficients for the problem and calibration samples, respectively, which depends on their respective chemical compositions. Besides, in Eq. (5), it has been considered that the thicknesses of the calibration and problem samples are the same, that is, $h$.

Furthermore, in Eq. (5) only the photons parallel to the symmetry axis are detected. However, the non-coaxial photons are also considered, being the angle between the photon trajectory and the coaxial axis of the detector very small. See [15,31,32] for further information about the conditions required in order to properly apply Eq. (5).

Therefore, the efficiency function calculated in the problem sample matrix, $\varepsilon\ (E_\gamma > 150\ \text{keV}, h, \eta)$, would be given in the following way:

$$\varepsilon(E_\gamma > 150\ \text{keV}, h, \eta) = f_a^C(E_\gamma > 150\ \text{keV}, h, \eta)\ \varepsilon_c(E_\gamma > 150\ \text{keV}, h) \quad (6)$$

where $\varepsilon_c(E_\gamma > 150\ \text{keV}, h)$ and $f_a^C(E_\gamma > 150\ \text{keV}, h, \eta)$ are the efficiency in the calibration matrix and the self-absorption correction factor, respectively, which are calculated for gamma energies higher than 150 keV.

Taking Eqs. (1) and (6), it is possible to determine both artificial and natural radionuclides contained in problem samples. Therefore, in

**Table 1**
External validation procedure of the general $\varepsilon_c(E_\gamma > 150\ \text{keV}, h)$ function in the case of artificial radionuclides contained in a soil sample (Soil-1), a milk powder sample (Milk powder), two water samples (Water-1 and Water-5), as well as another soil sample (Soil-2), that were employed in Inter-comparison – CSN/CIEMAT exercises carried out in 2016, 2018, 2019 and 2020, respectively.

| RN | $E_\gamma$(keV) | Water-1 | | | Water-5 | | | Milk powder | | |
|---|---|---|---|---|---|---|---|---|---|---|
| | | $a$ (Bq kg$^{-1}$) | Reference values (Bq kg$^{-1}$) | $z_{score}$ | $a$ (Bq kg$^{-1}$) | Reference values (Bq kg$^{-1}$) | $z_{score}$ | $a$ (Bq kg$^{-1}$) | Reference values (Bq kg$^{-1}$) | $z_{score}$ |
| $^{54}$Mn | 834.8 | 4.6(4) | 4.3(2) | 0.5 | 3.0(4) | 2.50(12) | 1.1 | | | |
| $^{59}$Fe | 1099.25 | 12.0(9) | 9.9(1.0) | 1.6 | 5.4(9) | 5.9(5) | −0.5 | | | |
| $^{60}$Co | 1173.20 | 5.0(4) | 4.79(18) | 0.5 | 2.0(4) | 2.10(7) | −0.2 | 29.0(8) | 26.8(1.0) | 1.7 |
| $^{65}$Zn | 1115.60 | 8.1(7) | 6.8(3) | 1.7 | 5.6(8) | 5.9(4) | −0.3 | | | |
| $^{134}$Cs | 795.8 | 1.9(4) | 1.92(19) | −0.2 | 1.7(4) | 1.8(2) | −0.1 | 49.5(1.1) | 48(2) | 0.7 |
| $^{137}$Cs | 661.8 | 3.4(3) | 3.3(2) | 0.5 | 1.2(4) | 1.55(7) | −0.9 | 14.9(5) | 14.0(6) | 1.2 |

| RN | $E_\gamma$(keV) | Soil-1 | | | Soil-2 | | |
|---|---|---|---|---|---|---|---|
| | | $a$ (Bq kg$^{-1}$) | Reference values (Bq kg$^{-1}$) | $z_{score}$ | $a$ (Bq kg$^{-1}$) | Reference values (Bq kg$^{-1}$) | $z_{score}$ |
| $^{54}$Mn | 834.8 | 10.9(4) | 10.3(6) | 0.8 | | | |
| $^{59}$Fe | 1099.25 | | | | 2.1(8) | 2.1(5) | 0.0 |
| $^{60}$Co | 1173.20 | 8.8(3) | 9.6(6) | −1.1 | 7.2(4) | 7.5(8) | −0.3 |
| $^{134}$Cs | 795.8 | 6.2(3) | 5.4(3) | 2.0 | 9.3(5) | 6.7(9) | 2.5 |
| $^{137}$Cs | 661.8 | 5.3(2) | 4.8(3) | 1.4 | 5.3(4) | 4.9(7) | 0.5 |

**Table 2**
External validation procedure of the general $\varepsilon_c(E_\gamma > 150$ keV, $h)$ function in the case of natural radionuclides ($^{40}$K) contained in $K_2CO_3$ sample, where the reference value for the $^{40}$K activity concentration is (17800 ± 255) Bq kg$^{-1}$. Besides, an internal validation was carried out varying the $K_2CO_3$ thickness ($h$). Besides, these results were compared with the ones obtained by the efficiency function, $\varepsilon_c^{RGK-1}(h)$, which resulted from the calibration in efficiency fixing $E_\gamma$ and varying $h$ using the RGK-1 standard.

| | $\varepsilon_c(E_\gamma > 150$ keV, $h)$ | | $\varepsilon_c^{RGK-1}(h)$ | |
|---|---|---|---|---|
| $h$ (mm) | $a$ (Bq kg$^{-1}$) | $z_{score}$ | $a$ (Bq kg$^{-1}$) | $z_{score}$ |
| 9.1 | 18,228 ± 499 | 0.8 | 17,462 ± 478 | −0.6 |
| 23.2 | 17,486 ± 415 | −0.6 | 17,472 ± 415 | −0.7 |
| 46.4 | 16,815 ± 400 | −2.1 | 16,767 ± 399 | −2.2 |

Tables 1–3, the validations related to $\varepsilon_c(E_\gamma > 150\ \text{keV}, h, \eta)$ have been carried out. For this, samples that contain artificial and natural radionuclides have been selected, where the results for the former radionuclide type have been shown in Table 1, while the ones corresponding to the latter type can be found in Tables 2 and 3. Therefore, as can be seen in Table 1, for all samples chosen, that is, Water-1, Water-5, Milk powder, Soil-1 and Soil-2, the obtained $|z_{score}|$ values were less than 2 in general, achieving a very good validation in the case of artificial radionuclides. Regarding the artificial radionuclides, decay corrections have been considered to calculate their activity concentrations, and information about their half-lives, $T_{1/2}$, as well as their gamma emission probabilities can be found in Table A.4 (see Supplementary Material).

In order to proceed with the previous validations, it was necessary to use the following equation to calculate the $z_{score}$ values:

$$z_{score} = \frac{a - a_r}{\sqrt{\sigma_a^2 + \sigma_a^2 r}} \tag{7}$$

where $a$ and $a_r$ are the calculated and reference activity concentrations, respectively, whose uncertainties given at 1 sigma level are $\sigma_a$ and $\sigma_{a_r}$, respectively. $z_{score}$ values in the range from −2 to 2 are considered good.

On the other hand, regarding the results obtained for natural radionuclides, in Tables 2 and 3, two cases have been distinguished. The case corresponding only to $^{40}$K for which the $K_2CO_3$ sample was chosen. Given that $^{40}$K has an only gamma emission (1460.83 keV), the $K_2CO_3$ sample thickness was varied, getting three $K_2CO_3$ samples whose $h$ values are well distributed throughout the $h$ range ($h$ = 9.1 mm, 23.2 mm and 46.4 mm), achieving to accomplish both external and internal validations at the same time. Furthermore, the calculations resulted from $\varepsilon_c(E_\gamma > 150$ keV, $h)$ have been compared with the ones obtained by the efficiency function, $\varepsilon_c^{RGK-1}(h)$. $\varepsilon_c^{RGK-1}(h)$ is the function obtained in [24] which resulted from the calibration in efficiency fixing $E_\gamma$ and varying $h$ by using the RGK-1 standard, while $\varepsilon_c(E_\gamma > 150$ keV, $h)$ was obtained varying $E_\gamma$ as was previously explained. As can be seen in Table 2, similar $z_{score}$ values were obtained for both efficiency functions.

There is only one case ($h$ = 46.4 mm) where $|z_{score}|$ was > 2. However, this is consistent since that $h$ value was very close to the upper limit of the selected $h$ range, that is, 50 mm. Therefore, a very good validation was achieved in the case of $^{40}$K by $\varepsilon_c(E_\gamma > 150$ keV, $h)$.

Then, in Table 3, the validation cases corresponding to the two soil samples (IAEA-326 and IAEA-327), as well as the one related to the furnace slag sample (Furnace slag), can be found. It is easy to realize that for all gamma energies, very good $z_{score}$ values were obtained excepting three $E_\gamma$ cases: 583 keV, 609 keV and 1120 keV. These three energies, where the first two energies belong to $^{214}$Bi and the third one corresponds to $^{208}$Tl, are clearly affected by the TCS effects and, consequently, TCS corrections are required. This is very consistent with the dissimilarities existing between the behavior of the $pr_i$ parameters obtained at these energies compared with the one related to the $pr_i$ values resulted from the fits done at other energies, this having been previously proven in Section 3.1. Therefore, in Section 3.2, a novel and simple methodology has been carried out in order to correct the TCS effects.

### 3.2. Corrections of the $\varepsilon_c(E_\gamma, h)$ function varying the distance: $\varepsilon_c(E_\gamma, h, d)$

Since TCS corrections are needed when the efficiency is calculated as a function on the energy, in this Section a practical and general method, which was previously described in Section 2.2, has been proposed for this correction type. Therefore, firstly, it is necessary to define the equations that have been employed to accomplish the proposed methodology. The efficiency function given by Eq. (4), $\varepsilon_c(E_\gamma, h)$, needs to be corrected by several correction factors when the distance, $d$, between the geometry bottom and the detector window is varied. Therefore, the resulted efficiency function, $\varepsilon_c(E_\gamma, h, d)$, can be calculated in the problem sample matrix, that is, $\varepsilon(E_\gamma, h, d, \eta)$, which is given by the following equation:

$$\varepsilon(E_\gamma, h, d, \eta) = f_a \varepsilon_c(E_\gamma, h, d) = f_T \varepsilon_c'(E_\gamma, h, d) = f_g f_s f_a \varepsilon_c'(E_\gamma, h, d) \tag{8}$$

where $f_g$ is the correction factor related to the geometry which only depends on the distance $d$, $f_s$ is the correction factor due to TCS effects, which depends on the energy, $E_\gamma$, problem sample thickness, $h$, the distance, $d$, and the density and mass attenuation coefficient of the calibration standard, $\rho_c$ and $\eta_c$, respectively, $f_a$ is the correction corresponding to the self-absorption effects, whose dependence was studied in Eq. (5), and $f_T$ is the total correction which involves the other three previous corrections. On the other hand, $\varepsilon_c'(E_\gamma, h, d)$ is obtained from $\varepsilon_c(E_\gamma, h)$ for each $d$ value, since the $h$ range covered by $\varepsilon_c(E_\gamma, h)$ goes from 5 mm to 45 mm in the case of the RGU-1 standard.

Then, two types of samples were chosen to carry out a much more complete study on the TCS corrections varying the distance ($d$). The RGU-1 standard and a tin concentrate sample (Sn-Sample) were selected for this study since their chemical compositions and densities are very different from each other, and their average atomic numbers, <Z>,

**Table 3**
External validation procedure of the general $\varepsilon_c(E_\gamma > 150$ keV, $h)$ function in the case of natural radionuclides contained in the soil samples IAEA-326 and IAEA-327, and a furnace slag sample which was used in an Inter-comparison – CSN/CIEMAT exercise carried out in 2019.

| | | IAEA-326 | | | IAEA-327 | | | Furnace slag | | |
|---|---|---|---|---|---|---|---|---|---|---|
| RN | $E_\gamma$(keV) | $a$ (Bq kg$^{-1}$) | Reference values (Bq kg$^{-1}$) | $z_{score}$ | $a$ (Bq kg$^{-1}$) | Reference values (Bq kg$^{-1}$) | $z_{score}$ | $a$ (Bq kg$^{-1}$) | Reference values (Bq kg$^{-1}$) | $z_{score}$ |
| $^{226}$Ra | 185.96 | 35(3) | | 0.6 | 38(5) | | 0.7 | 107(8) | 106.3(1.7) | 0.1 |
| $^{214}$Pb | 295.22 | 29.8(9) | | −0.9 | 35(2) | | 0.3 | 103(3) | | −0.9 |
| | 351.93 | 30.1(8) | 33(3) | −0.8 | 36(2) | 34(3) | 0.5 | 104(3) | | −0.7 |
| $^{214}$Bi | 609.31 | 25.5(7) | | −2.2 | 26.3(1.1) | | −1.9 | 86(2) | | −7.1 |
| | 1120.29 | 26.3(1.4) | | −1.8 | 31(3) | | −0.3 | 79(4) | | −6.5 |
| $^{228}$Ac | 338.42 | 40(7) | 40(2) | 0.0 | 43(8) | 39(3) | 0.5 | 131(22) | 130(5) | 0.0 |
| | 911.16 | 38.8(1.2) | | −0.5 | 42(2) | | 1.0 | 134(4) | | 0.8 |
| $^{212}$Pb | 238.63 | 38.2(9) | 39.1(1.7) | −0.5 | 37.7(1.1) | 38.2(1.8) | −0.2 | 140(3) | | 1.7 |
| $^{208}$Tl | 583.19 | 30.5(9) | | −4.5 | 30.1(1.5) | | −4.0 | 109(3) | | −3.6 |
| $^{40}$K | 1460.83 | 591(13) | 580(28) | 0.4 | 660(17) | 621(27) | 1.2 | 148(5) | 161(6) | −1.6 |

belong to the low and high <Z> range, that is, <Z> ≤ 26 and <Z> > 26, respectively. The apparent density and <Z> values were approximately 1.63 g cm$^{-3}$ and 3.54 g cm$^{-3}$, and 13 and 50 in the cases of RGU-1 and Sn-Sample, respectively. See [15] for further information about the criteria followed in order to establish the limits of each <Z> range.

On the other hand, since RGU-1 and Sn-Sample are samples whose activity concentrations are known, the corrected efficiencies given by Eq. (8) can be calculated for each selected $d$ value (0, 25, 35, 45, 55 and 65 mm) using Eq. (1), where the sample thickness has been fixed at $h$ = 25 mm. Consequently, the corrected efficiencies, provided by Eq. (8), can be given by the following functions: $\varepsilon_c(E_\gamma, d)$ and $\varepsilon(E_\gamma, d, \eta)$ for the calibration and problem sample matrices, respectively, since $h$ is fixed. Besides, the non-corrected efficiency, which was also shown in Eq. (8), that is, $\varepsilon_c'(E_\gamma, h, d)$, can be given by the $\varepsilon_c'(E_\gamma, d)$ function because of the same previous reason. Then, it is necessary to clarify that Sn-Sample has been considered as a sample whose activity concentrations are known because it was measured by the XtRa taking five aliquots of this sample. Therefore, since the XtRa calibration has been fully validated [24], it is possible to classify Sn-Sample as a sample whose activity concentrations are known. The reference activity concentration values are 4989(58) Bq kg$^{-1}$ and 1270(17) Bq kg$^{-1}$ for all radionuclides belonging to the $^{238}$U- and $^{232}$Th-series, respectively, because it has been checked that they are in secular equilibrium.

As can be seen in Fig. 3, two cases have been considered to carry out the $\varepsilon_c'(E_\gamma, d)$ corrections: graphics from 3A to 3C show the corrections done using the RGU-1 standard, and from graphics 3D to 3G, the ones corresponding to the case employing the Sn-Sample can be found. For the first case, it is possible to observe that all $E_\gamma$ values that were not affected by TCS effects (let us call N-TCS energies), that is, 46 keV, 63 keV, 186 keV, 242 keV, 295 keV and 352 keV, can be corrected by a very similar factor value, that is, the geometrical correction factor, $f_g$ (see graphic 3A). Therefore, the correction provided by $f_g$ function is completely known since it only depends on $d$.

On the other hand, in Fig. 3 (graphic 3B), it is possible to observe that the total corrections, that is, $f_g \times f_s$, done for all energies different from N-TCS energies, which let us call TCS energies, were dissimilar. This is very consistent because the TCS energies (609 keV, 768 keV, 934 keV, 1120 keV and 1238 keV which all belong to $^{214}$Bi) are affected by TCS effects and, consequently, each one of those energies is corrected by a different $f_s$ value. Besides, it is interesting to realize that some energies such as 1120 keV and 1238 keV can be corrected more easily than other energies like 609 keV and 934 keV. This makes that this TCS correction method is very useful to identify which $E_\gamma$ are affected more significantly by TCS effects. Moreover, in graphic 3B, note that as $d$ increases, the TCS effects are less significant and, consequently, the TCS energies become N-TCS energies, making the correction given by $f_s$ tend to be 1 at $d$ = 65 mm. This is very consistent since as $d$ increases, the absolute efficiency ($\varepsilon_{ab}$) decreases and, consequently, a diminution of the TCS effects is occasioned because $\varepsilon_{ab}$ and TCS are related to each other [32]. On the other hand, as can be seen in graphics 3A and 3B, fits of the corrections were provided to prove the physical meaning of them:

$$\left(f_g \times f_s\right)^k = a_{T1}^k \exp\left(a_{T2}^k d\right) + a_{T3}^k \tag{9}$$

where $a_{Tj}^k$ (with j = 1, 2, 3) are the parameters resulted from the $\left(f_g \times f_s\right)^k$ fits versus $d$, and $k$ = low <Z> or high <Z> to distinguish between the parameters obtained after the correction fits provided for the low <Z> and high <Z> sample cases, that is, RGU-1 and Sn-Sample, respectively. In Table A.5 (see Supplementary Material), the $a_{Tj}^{low<Z>}$ parameters have been shown, where the relative average residual values, <Residual> (%), obtained after each fit were less than 2.4% in

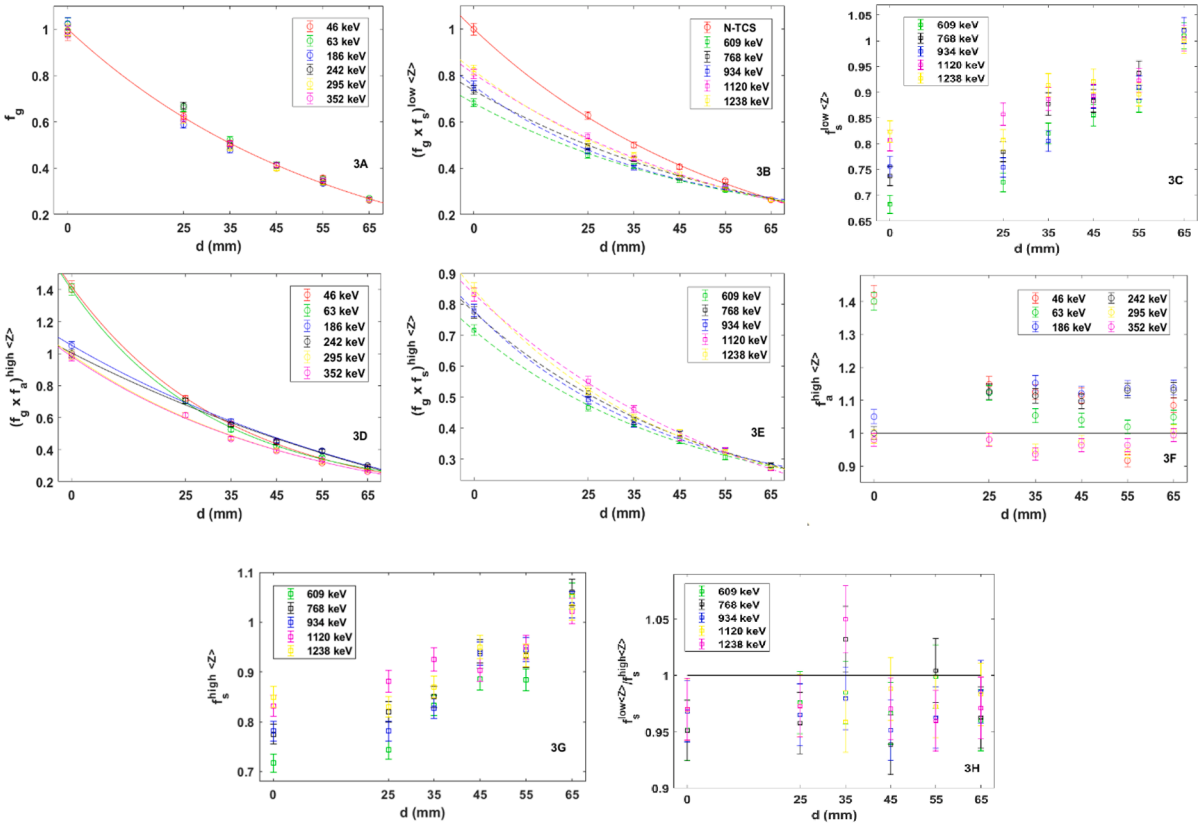


**Fig. 3.** From 3A to 3C: $f_g$ and $f_s$ factors corresponding to the N-TCS and TCS energies when the sample <Z> is low; From 3D to 3G: $f_g$, $f_s$ and $f_a$ factors corresponding to the N-TCS and TCS energies when the sample <Z> is high, and 3H is a comparison between $f_s^{low<Z>}$ and $f_s^{high<Z>}$. This study has been done varying the distance between the geometry bottom and the detector window, $d$, and fixing the sample thicknesses at $h$ = 25 mm.

general. Therefore, very good fits carried out for $\left(f_g \times f_s\right)^{low<Z>}$ were done.

Then, regarding the graphic 3C, the correction given by the $f_s$ factor has been plotted versus $d$ for TCS energies. It was possible to determine $f_s$ function for RGU-1 standard since the $\left(f_g \times f_s\right)^{low<Z>}$ and $f_g$ functions were previously obtained. The differences explained above with respect to the dissimilar TCS corrections depending on $E_\gamma$ can be seen more clearly in graphic 3C.

Once the cases corresponding to the low <Z> sample (RGU-1 standard) have been analyzed, the resulted corrections for the high <Z> sample (Sn-Sample) were considered below, which have been shown in Fig. 3 (graphics from 3D to 3G). In graphics 3D and 3E, it is possible to observe the total corrections provided for N-TCS and TCS energies, respectively. In graphic 3D, the corrections given by $\left(f_g \times f_a\right)^{high<Z>}$ for N-TCS energies were clearly very similar at all these energies excepting for 46 keV and 63 keV, being this difference greater as $d$ decreases. Therefore, given that in order to calculate the activity concentrations for each $d$ value, the self-absorption corrections provided by the Cutshall's model have been considered, $\left(f_g \times f_a\right)^{high<Z>}$ values should be very similar regardless of the selected N-TCS energy and they should tend to be 1. In other words, the $f_a$ function, shown in Eq. (8), can be written in the following way:

$$f_a = \frac{f_a^{real}}{f_a^C} \tag{10}$$

where $f_a^C$ is the self-absorption correction provided by the Cutshall's model, which was given by Eq. (5), and $f_a^{real}$ is the self-absorption correction that should be obtained, that is, the real correction which needs to be considered in order to properly correct the self-absorption effects.

To observe more clearly the $f_a$ function behavior, $f_a$ values have been plotted versus $d$ in Fig. 3 (graphic 3F). As can be seen in this graphic, the self-absorption corrections provided by the Cutshall's model are not good for 46 keV and 63 keV at $d = 0$ and, consequently, for this $d$ value, $f_a^C$ function is not working at low energies for high <Z> samples. This fact is very consistent, since one of the requirements for $f_a^C$ is the need for parallelism between the travel direction of the emitted photons and the coaxial detector axis [31–33]. Therefore, for high <Z> samples and low energies at $d = 0$, this requirement is not being fulfilled. However, note that in graphic 3F, as $d$ increases, the $f_a$ values obtained for low energies were closer to 1. This is very reasonable because as $d$ increases, the solid angle decreases and, therefore, the previous parallelism condition is easier to be fulfilled. Consequently, the methodology proposed in this work to correct TCS effects is very useful to be employed in order to make the $f_a^C$ function work properly. In Section 3.4, this methodology proposed to use $f_a^C$ in a proper way has been studied in depth.

On the other hand, regarding the corrections carried out by the $\left(f_g \times f_a\right)^{high<Z>}$ function, previously mentioned in Fig. 3 (graphic 3D), fits were accomplished for these corrections, having employed the function described in Eq. (9). Besides, the parameters, $a_{Tj}^{high<Z>}$ (with j = 1, 2, 3), and the <Residual> values resulted from these fits for N-TCS energies can be found in Table A.6 (see Supplementary Material), where the obtained <Residual> values were less than 4.5%.

With respect to the cases corresponding to the TCS energies for Sn-Sample, the corrections were shown in Fig. 3 (graphics 3E and 3G). In graphic 3E, the total corrections can be found, which were given by $\left(f_g \times f_s\right)^{high<Z>}$. Note that in this case, $f_a$ was considered to be 1 in order to make easier the obtaining of the $f_s^{high<Z>}$ function. This approximation for $f_a$ is very reasonable because in graphic 3F, it is possible to observe that $f_a$ was very close to 1 at $E_\gamma = 352$ keV. Consequently, since the lowest $E_\gamma$ value belonging to the TCS energies is 609 keV, considering $f_a$ 1 is a very good approximation in this case (relative differences of $f_a$ from 1 less than 5%). By using the $\left(f_g \times f_s\right)^{high<Z>}$ function, which was shown in graphic 3E, it was possible to calculate the corrections provided by $f_s^{high<Z>}$, which were plotted versus $d$ in graphic 3G. As can be seen in graphic 3G, the corrections carried out by $f_s^{high<Z>}$ were not the same than the ones resulted from the case studied in graphic 3C, being these differences more significant for 768 keV, 934 keV and 1120 keV. The reason is because for these $E_\gamma$, energies lower than 150 keV are involved in the TCS effects and, consequently, the chemical composition of the selected sample is influencing the correction provided by $f_s$, which can be easily checked in graphic 3H where $f_s^{low<Z>}/f_s^{high<Z>}$ was plotted versus $d$. This agrees with previous studies [34,35]. However, note that as can be seen in graphics 3C and 3G, these differences between the TCS corrections accomplished for the two samples (RGU-1 and Sn-Sample) became less significant as $d$ increases (see graphic 3H). This occurs in this way because since as $d$ value increases, TCS effects are less relevant and, consequently, the $f_s$ dependence on chemical sample composition can be neglected.

On the other hand, it is very interesting to realize that in graphics 3C and 3G, the TCS corrections obtained for 609 keV were higher than the ones resulted for the cases corresponding to 1120 keV. This agrees very well with the $z_{score}$ values shown in Table 3 (see Section 3.1), where the $|z_{score}|$ values obtained for 609 keV were worse than the ones resulted for 1120 keV, which is due to the TCS effects being more relevant for the first gamma emission energy than for the second one.

Regarding the fits done for the obtained $\left(f_g \times f_s\right)^{high<Z>}$ values, the function previously defined by Eq. (9) was chosen. In Table A.7 (see Supplementary Material), the $a_{Ti}^{high<Z>}$ parameter values resulted from the $\left(f_g \times f_s\right)^{high<Z>}$ fits can be found, as well as their obtained <Residual> values, which were less than 3.6% (see [34] for further information about the equation employed to obtain <Residual>).

After this comprehensive study carried out in Section 3.2, the methodology is used to determine a general efficiency function, $\varepsilon_c(E_\gamma, d)$, which will be employed to correct TCS effects. Then, the methodology proposed in Section 3.2 is also employed to properly correct self-absorption effects by $f_a^C$ (Section 3.4).

### 3.3. TCS corrections varying the d distance: obtaining and validation of the $\varepsilon_c(E_\gamma, d)$ function

In this Section, a study on the TCS corrections varying the $d$ distance has been accomplished. For this, the methodology previously described in Section 2.2 (methods) has been employed, which consists of calibrating the XtRa detector varying the $d$ distance in this case. The RGU-1 standard was selected and compacted until reaching a thickness value, $h$, of 25 mm, and it was measured at each selected $d$ value: 0, 25, 35, 45, 55 and 65 mm, the $h$ value being 25 mm for all cases. In this efficiency calibration, the following gamma emission energies were chosen: 46 keV, 63 keV, 186 keV, 242 keV, 295 keV, 352 keV, 609 keV, 768 keV, 934 keV, 1120 keV and 1238 keV.

Therefore, once the $\varepsilon_c$'$(E_\gamma, h, d)$ corrections were accomplished by the corrections previously provided in Eq. (8), the corrected experimental *FEPE* values were plotted versus $E_\gamma$ for each $d$ value in order to obtain a general efficiency function in the calibration matrix, $\varepsilon_c(E_\gamma, d)$ (see Fig. 4). As can be seen in Fig. 4, the corrected experimental *FEPE* values as well as their fits were shown versus $E_\gamma$ for each $d$ distance, where the fitting function proposed in this case is given by the following equation:

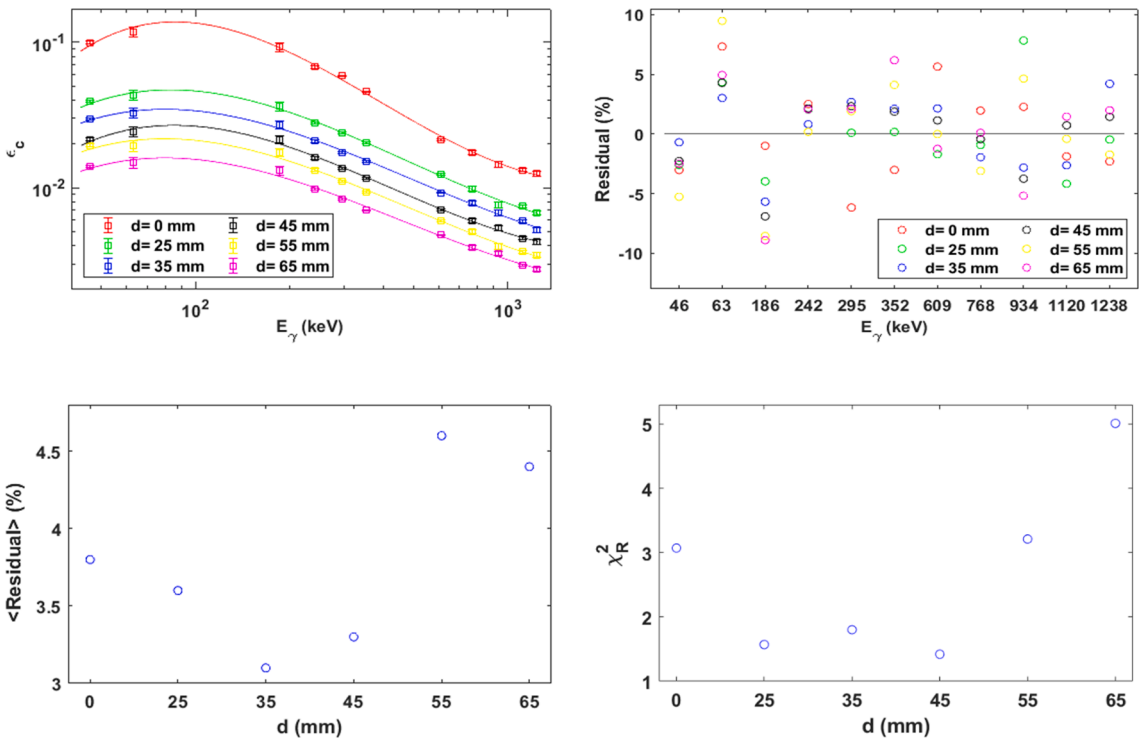


**Fig. 4.** Fits of the corrected efficiency, $\varepsilon_c$, versus $E_\gamma$, using logarithmic scale, for each $d$ value and fixing the thickness of the calibrating sample (RGU-1) at 25 mm. Then, the relative residuals and relative average residuals, as well as $\chi^2_R$ values obtained for each $d$ value have been shown.

$$ln\left(\varepsilon_c\left(E_\gamma,h,d\right)\right)=\sum_{i=1}^{4}b_i\ ln\left(E_\gamma/E_0\right)^{i-1} \tag{11}$$

where $b_i$ are the parameters resulted from the corrected *FEPE* fits, $E_0=1$ keV, $E_\gamma$ is the gamma energy, $h$ is the standard thickness which was fixed at 25 mm for all cases and $d$ is the distance between the geometry bottom and the detector window. Note that in Fig. 4, the energies belonging to low energy range (46 keV and 63 keV) were considered in order to fit the corrected experimental *FEPE* values. The reason was because of having an adequate number of *FEPE* values and, consequently, proper fits were provided by $\varepsilon_c(E_\gamma,d)$. On the other hand, it is necessary to clarify that since the obtention of $\varepsilon_c(E_\gamma>150$ keV, $h)$ (see Section 3.1) was carried out at $d=0$, it is possible to calculate the efficiency values at 46 keV ($^{210}$Pb) and 63 keV ($^{234}$Th) by using the other efficiency function $\varepsilon_c(h)$, which was obtained by varying $h$ and fixing $E_\gamma$ for natural radionuclides. Consequently, in the case of the $\varepsilon_c(E_\gamma>150$ keV, $h)$, it was not necessary to consider the 46 keV and 63 keV points to proceed with the fits, since at these energies, the efficiency values can perfectly be provided by $\varepsilon_c(h)$.

Therefore, after obtaining the $\varepsilon_c(E_\gamma,d)$ function at each $d$ value, where the resulted $b_i$ parameter values for each $d$ value can be consulted in Table A.9 shown in Supplementary Material, it was necessary to decide on what $d$ distance was the optimum value for $\varepsilon_c(E_\gamma,d)$. For this, an analysis on the relative residual and reduced chi-square ($\chi^2_R$) values obtained after each fit was carried out. In Fig. 4, it is possible to observe the relative residuals calculated for each $E_\gamma$ and $d$ values. Furthermore, when averaging the relative residuals obtained for each $d$ over all $E_\gamma$ values, the relative average residuals, <Residual>, can be known for each $d$. In Fig. 4, <Residual> and $\chi^2_R$ values calculated for each $d$ can also be found. In our case, the critical $\chi^2_R$ value was 2.01 at 0.05 significance level, since 7 degrees were obtained (see [36] for further information about tabulated $\chi^2_R$ values). Therefore, after analyzing the resulted $\chi^2_R$ values plotted in Fig. 4, it was possible to reduce the number of the possible $d$ values to three, that is, 25, 35 and 45 mm, which were the only cases whose $\chi^2_R$ values were less than the one considered as critical. Consequently, in order to be able to decide on what $d$ value is the most appropriate, <Residual> values were employed, $d=35$ mm being the $d$ value whose <Residual> was lower than the ones obtained for the other two $d$ value. Therefore, $d=35$ mm was considered as the optimum $d$ value for the $\varepsilon_c(E_\gamma,d)$ function. In Tables A.8 and A.9, it is also possible to find the corrected experimental efficiency values obtained, and the <Residual> and $\chi^2_R$ values resulted from each fit provided by $\varepsilon_c(E_\gamma,d)$ at each $d$ value, respectively.

On the other hand, validations of the $\varepsilon_c(E_\gamma,d)$ function for $d=35$ mm were carried out. For this, several problem samples were chosen: a seaweed sample (IARMA-097), three water samples (IARMA-098, IARMA-099 and IARMA-100), as well as mixtures of IAEA-375 with 52.5% of Sn-Sample (IAEA-375 + 52.5% Sn-Sample). As can be seen in Table 4, very good $z_{score}$ values were obtained for all artificial radionuclides contained in those five samples. Besides, in the case of the natural radionuclides, all $z_{score}$ values were also less than 2, even for 583 keV, 609 keV and 1120 keV, for which the $z_{score}$ values were −1.7, −0.9 and −0.3, respectively, in the case of IAEA-375 + 52.5% Sn-Sample. For these two same energies, the $z_{score}$ values obtained in Section 3.1.1 were bad because the TCS effects are much more significant when the $\varepsilon_c(E_\gamma,h)$ function is employed. Consequently, the $\varepsilon_c(E_\gamma,d)$ function obtained for $d=35$ mm can be used for artificial and natural radionuclides to correct the TCS effects and obtain very good results for both radionuclide types.

### 3.4. Methods to properly correct self-absorption effects by $f_a^C$ function when high <Z> samples are considered

As explained in Section 3.2, the self-absorption corrections provided by $f_a^C$ (defined in Eq. (5)) do not work in an adequate way when these corrections are applied to determine radionuclides contained in high <Z> samples. Therefore, in this Section, several methods were proposed to make the corrections given by $f_a^C$ work in a proper way. For this, a Sn-Sample, whose apparent density and <Z> are high, was selected. Furthermore, to test the corrections provided by $f_a^C$, a gamma energy

**Table 4**
External validation procedure of the general $\varepsilon_c(E_\gamma, d = 35$ mm) function in the case of artificial radionuclides contained in a seaweed sample (IARMA-097) and three water samples (IARMA-098, IARMA-099 and IARMA-100), that were employed in Inter-comparison – IARMA exercise carried out in 2020. Besides, external validations were applied in the case of the natural radionuclides, selecting for this, the mixture of IAEA-375 with 52.5% of the Sn-Sample (IAEA-375 + 52.5% Sn-Sample).

| RN | $E_\gamma$(keV) | IARMA-097 $a$ (Bq kg$^{-1}$) | IARMA-097 Reference values (Bq kg$^{-1}$) | IARMA-097 $z_{score}$ | IARMA-098 $a$ (Bq kg$^{-1}$) | IARMA-098 Reference values (Bq kg$^{-1}$) | IARMA-098 $z_{score}$ | IARMA-099 $a$ (Bq kg$^{-1}$) | IARMA-099 Reference values (Bq kg$^{-1}$) | IARMA-099 $z_{score}$ |
|---|---|---|---|---|---|---|---|---|---|---|
| $^{57}$Co | 122.06 | 4.9(3) | 4.8(3) | 0.2 | 0.82(15) | < 1 | – | 2.23(11) | 2.70(14) | −1.7 |
| $^{60}$Co | 1173.20 | 8.4(4) | 7.1(5) | 1.9 | 2.53(18) | 2.40(10) | 0.5 | 3.9(2) | 3.8(2) | 0.1 |
| $^{133}$Ba | 356.0 | 7.8(3) | 8.3(4) | −0.6 | 2.70(19) | 3.20(13) | −1.6 | 4.5(2) | 5.1(3) | −1.3 |
| $^{134}$Cs | 795.8 | 15.7(4) | 14.8(7) | 0.6 | 4.4(2) | 4.3(2) | 0.1 | 6.7(3) | 6.6(3) | 0.1 |
| $^{137}$Cs | 661.8 | 6.6(3) | 6.3(3) | 0.5 | 3.29(19) | 2.90(12) | 1.3 | 4.7(2) | 4.2(2) | 1.2 |
| $^{152}$Eu | 344.3 | 9.6(6) | 9.0(4) | 0.7 | 1.9(4) | 1.90(10) | 0.2 | 4.0(4) | 3.7(2) | 0.7 |
| $^{241}$Am | 59.54 | 9.1(3) | 8.0(3) | 1.3 | 4.1(2) | 3.70(15) | 1.2 | 8.6(3) | 7.5(3) | 1.5 |

| RN | $E_\gamma$(keV) | IARMA-100 $a$ (Bq kg$^{-1}$) | IARMA-100 Reference values (Bq kg$^{-1}$) | IARMA-100 $z_{score}$ | RN | $E_\gamma$(keV) | IAEA-375 + 52.5% Sn-Sample $a$ (Bq kg$^{-1}$) | IAEA-375 + 52.5% Sn-Sample Reference values (Bq kg$^{-1}$) | IAEA-375 + 52.5% Sn-Sample $z_{score}$ |
|---|---|---|---|---|---|---|---|---|---|
| $^{54}$Mn | 834.8 | | | | $^{234}$Th | 63.29 | 2772(139) | 2630(31) | 1.0 |
| $^{57}$Co | 122.06 | 0.36(2) | < 1 | – | $^{226}$Ra | 185.96 | 3055(244) | 2629(31) | 1.7 |
| $^{59}$Fe | 1099.25 | | | | $^{214}$Pb | 295.22 | 2491(125) | | −1.1 |
| $^{60}$Co | 1173.20 | 4.9(3) | 4.8(2) | 0.2 | | 351.93 | 2461(123) | | −1.3 |
| $^{133}$Ba | 356.0 | 8.1(3) | 9.0(4) | −1.0 | $^{214}$Bi | 609.31 | 2512(126) | | −0.9 |
| $^{134}$Cs | 795.8 | 5.5(3) | 5.1(2) | 0.7 | | 1120.29 | 2589(129) | | −0.3 |
| $^{137}$Cs | 661.8 | 10.6(3) | 9.5(4) | 1.2 | $^{228}$Ac | 338.42 | 620(31) | 677(9) | −1.7 |
| $^{152}$Eu | 344.3 | 10.1(6) | 9.2(5) | 0.9 | | 911.16 | 730(37) | | 1.4 |
| $^{241}$Am | 59.54 | 10.5(5) | 10.0(4) | 0.5 | $^{212}$Pb | 238.63 | 745(37) | 677(9) | 1.8 |
| | | | | | $^{208}$Tl | 583.19 | 622(31) | | −1.7 |

belonging to the low energy range (< 150 keV) was selected, that is, $E_\gamma$ = 63 keV ($^{234}$Th).

Firstly, several Sn-Sample thicknesses, $h$, were taken: 3, 6, 12, 24 and 48 mm, which are well distributed throughout the thickness range used in the XtRa calibration. Besides, in this first case, the $d$ value was fixed at 0 mm, that is, right above the detector window. Therefore, it was possible to check for which Sn-Sample $h$ range, the corrections given by $f_a^C$ were valid. To proceed with this test, $z_{score}$ were calculated for each $h$ value at $E_\gamma$ = 63 keV, which can be found in Fig. 5 (graphic 5A). As can be seen in graphic 5A, the $z_{score}$ values were very good for small $h$ values, that is, $h$ values less than 12 mm. From $h$ = 12 mm, the self-absorption effects became very important and, consequently, the corrections provided by $f_a^C$ are not valid. Therefore, it is recommendable to select small $h$ values when samples, whose density and <Z> are very high, are

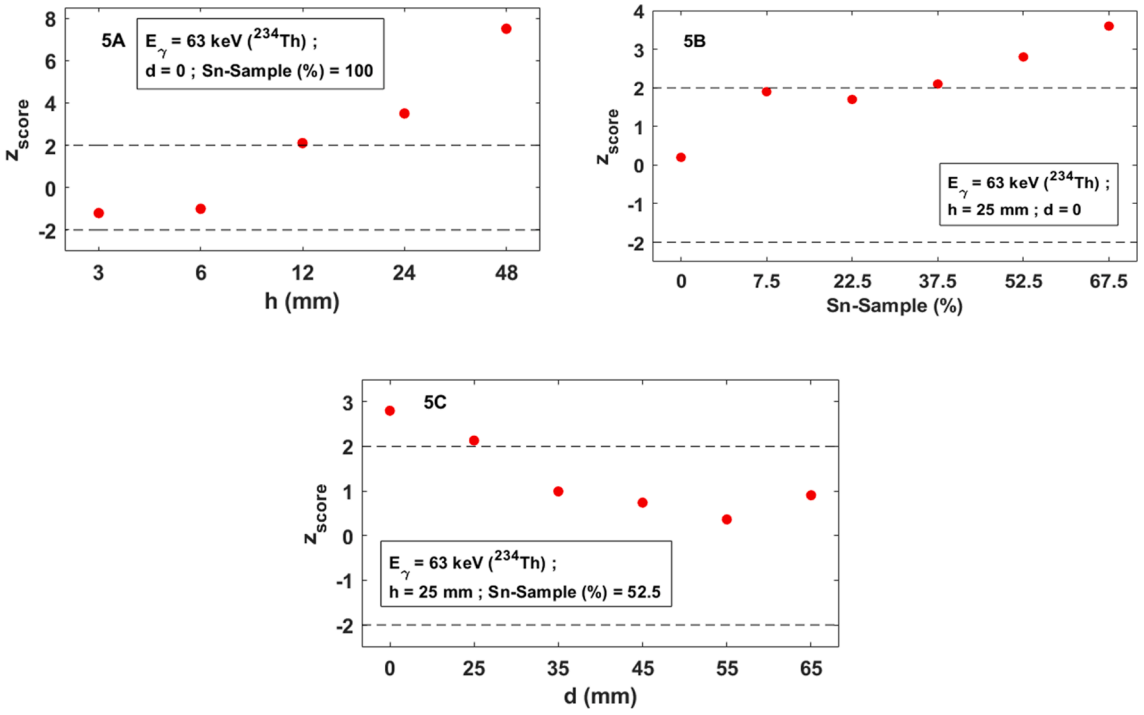


**Fig. 5.** 5A and 5B: Study on the validity of the self-absorption corrections. For this, the $z_{score}$ value was obtained when the Sn-Sample thickness and the Sn-Sample proportion in the mixture with IAEA-375 are increased, respectively, where $h$ was fixed at 25 mm in graphic 5B, $d$ value being zero in both graphics; 5C: Study on the improvement of the self-absorption corrections when the distance $d$ is increased. This study was done taking the mixture IAEA-375 with Sn-Sample fixing $h$ at 25 mm, where the proportion of the latter is constant and equal to 52.5%.

measured by using gamma spectrometry, making the self-absorption effects much less significant.

On the other hand, the Sn-Sample was mixed with a soil sample (IAEA-375) to test the validity of $f_a^C$ when the proportion of the Sn-Sample is varied. Several proportions (given in %) of Sn-Sample were chosen: 0, 7.5, 22.5, 37.5, 52.5 and 67.5. In these cases, the thickness value used to prepare the mixtures between Sn-Sample and IAEA-375 was $h = 25$ mm, where $d$ is zero for all of them. In Fig. 5 (graphic 5B), the $z_{score}$ values were obtained for each Sn-Sample proportion. Therefore, as can be seen in graphic 5B, the validity of $f_a^C$ was not good when the Sn-Sample proportion began to be relevant, that is, from 37.5%. Besides, since the $f_a^C$ function depends on the sample mass attenuation coefficient, $\eta$, it was calculated to find the $\eta$ value for which the corrections provided by $f_a^C$ start to be improper. The obtained $\eta$ value was 1.59 $cm^2\ g^{-1}$, this $\eta$ value being very similar with the one calculated in previous works on well-type Ge detectors, where the validity of the self-absorption corrections was also tested [34]. In the case of the well-type Ge detectors, the self-absorption corrections provided by the Appleby's model were taken [37], obtaining a critical $\eta$ value of 1.52 $cm^2\ g^{-1}$ at $E_\gamma$ = 63 keV ($^{234}$Th), which proves that both self-absorption correction models, Cutshall's and Appleby's models, have behaviors very similar.

Then, one of the mixtures previously employed in graphic 5B was selected for the study of the validity of the corrections given by $f_a^C$ varying $d$. For this, the mixture characterized by having 52.5% of Sn-Sample was used, where $h$ was fixed at 25 mm ($h$ value used in Section 3.3). This Sn-Sample percentage was selected instead of, e.g., 37.5%, in order to check in a more appropriate way how the $d$ distance variation influence the validity of the self-absorption corrections provided by the Cutshall model. In Fig. 5 (graphic 5C), it is possible observe what happens when $d$ is varied. Therefore, as can be seen in graphic 5C, as $d$ value was increased, the $z_{score}$ values were better, achieving $z_{score}$ values less than 2 from $d = 35$ mm. Consequently, the conditions, that are required to properly use $f_a^C$, are fulfilled from $d = 35$ mm. This agrees with the results previously obtained in graphic 3F (see Fig. 3), which was shown in Section 3.2.

### 3.5. Dead time corrections by varying the d distance

After having proved that $\varepsilon_c$ ($E_\gamma$, $d = 35$ mm) is the function that best corrects TCS effects, a study on the dead time corrections was accomplished in this Section by using the same methodology which was employed in Section 3.3 in order to correct TCS effects. Three scale samples (Scale-A, Scale-B and Scale-C) were selected for this study, which were characterized by being very active and whose thicknesses were 25 mm for the three cases. The reason why very active samples were chosen was because as the activity concentration of a sample increases, the dead time increases, since a larger number of events are not detected. Considering this reasoning, it is possible to define the equation for the dead time, $t_d$, which can be experimentally calculated in the following way:

$$t_d^{exp}(\%) = 100(t_r - t_l)/t_r \tag{12}$$

where $t_d^{exp}$ is the dead time obtained experimentally by Eq. (12), and $t_r$ and $t_l$ are the real and live times, respectively, the former being the total time interval during which the events should be recorded, and the latter is the time interval for which the events have been truly recorded.

In order to carry out this study, the dead time values resulted from each scale sample, were plotted versus $d$ in Fig. 6. In this figure, it is possible to observe how the experimental dead time, $t_d^{exp}$, was reduced as the $d$ distance was increased. As can be seen in this figure, Scale-B was clearly the most active sample since the $t_d^{exp}$ values for this scale were the highest ones obtained for all selected $d$ values, where the $t_d^{exp}$ values were reduced from approximately 60% ($d = 0$) to 10% ($d = 65$ mm). Making use of this same reasoning in order to deduce which scale sample contains radionuclides whose activity concentrations are higher, it is possible to realize that Scale-C and Scale-A were the second and third most active scales, respectively, for which the $t_d^{exp}$ values were reduced approximately from 47% ($d = 0$) to 6% ($d = 65$ mm) and from 32% ($d = 0$) to 4% ($d = 65$ mm), respectively. Besides, it is necessary to clarify that the uncertainties associated to $t_d^{exp}$ were not taken into account because of being completely negligible. In order to correct the dead time, the method proposed in this Section has been successful, obtaining $t_d^{exp}$ reductions of up to 50% for the three selected scale samples.

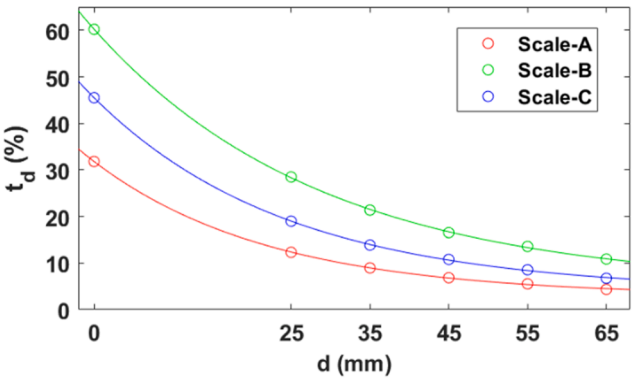


**Fig. 6.** Dead-time corrections carried out varying the distance $d$ from 0 to 65 mm for three scale samples (Scale-A, Scale-B and Scale-C), whose thicknesses have been fixed at 25 mm, including fits done for these dead-time corrections.

Taking the $t_d^{exp}$ values plotted versus $d$ in Fig. 6, it is possible to observe that they have a clear tendence, proving their physical meaning. Therefore, fits of $t_d^{exp}$ versus $d$ was carried out for each scale type in order to verify their physical meaning. For this, the following equation was selected:

$$t_d(\%) = c_1 \exp(c_2 d) + c_3 \tag{13}$$

where $c_i$ (with i = 1, 2, 3) are the parameters resulted from the fits provided by the theoretical dead time function, $t_d$, versus the $d$ distance, which were shown in Table A.10 (see Supplementary Material), where the <Residual> values obtained for each fit were less than 2%.

## 4. Conclusions

In the present work, a general efficiency function, $\varepsilon_c(E_\gamma, h)$, has been obtained in order to determine artificial and natural radionuclides. For this, a novel method has been proposed in this study which consists of calibrating the detector (in our case, XtRa), fixing and varying the selected gamma energies ($E_\gamma$) and standard thicknesses ($h$), respectively. Taking the parameters resulted from fitting the experimental *FEPE* versus $h$, $pr_i(E_\gamma)$, they are fitted, in turn, versus $E_\gamma$. To proceed with the method proposed to obtain $\varepsilon_c(E_\gamma, h)$, standards which contain only natural radionuclides were used for the calibration. This makes this method be very useful given that it allows us to determine artificial radionuclides without needing to calibrate by using point sources that contain the desired artificial radionuclides.

The $\varepsilon_c(E_\gamma, h)$, considering only high energies, that is, $\varepsilon_c(E_\gamma > 150$ keV, $h)$, was validated for several sample types which contain artificial and natural radionuclides. Regarding the validations carried out for samples that contain only artificial radionuclides, very good $|z_{score}|$ values were obtained which were less than 2 for all cases. For the other samples that contain natural radionuclides, very good $z_{score}$ values were obtained for all radionuclides, except for $^{214}$Bi (609 keV and 1120 keV) and $^{208}$Tl (583 keV). Since those three gamma energies are affected by TCS effects, a method was proposed in order to carry out TCS corrections. This method consisted of recalibrating the XtRa detector varying the sample-detector distance, $d$, and fixing the thickness standard, $h$, obtaining a

general efficiency function, $\varepsilon_c(E_\gamma, d)$. For this, it was necessary to check the behavior of the efficiency corrections depending on the sample type in order to assure how different these corrections are depending on the selected sample. Therefore, two samples were chosen (RGU-1 and Sn-Sample), whose densities and chemical compositions are very different from each other. It was possible to observe that for those two samples, the TCS effects were corrected as $d$ increased. Moreover, it was found that the TCS corrections were different in the cases of RGU-1 and Sn-Sample, since sometimes $E_\gamma$ values less than 150 keV are involved in the TCS effects. However, these differences were decreased as $d$ increased, since as $d$ increased, the TCS effects were less significant.

Regarding the method proposed to correct the TCS effects, several $d$ values were chosen (from 0 to 65 mm), and the RGU-1 standard was employed whose thickness was fixed at 25 mm. The corrected experimental *FEPEs* were fitted versus $E_\gamma$ for each $d$, demonstrating that for $d =$ 35 mm, the fitting function, $\varepsilon_c(E_\gamma,\ d = 35\ \text{mm})$ provided the best fit. Then, $\varepsilon_c(E_\gamma,\ d = 35\ \text{mm})$ was validated for several samples, achieving very good $z_{score}$ for artificial and natural radionuclides, even in the cases of $E_\gamma = 583$ keV, 609 keV and 1120 keV. Regarding the possible systematic errors associated to the results provided by $\varepsilon_c(E_\gamma,\ d = 35\ \text{mm})$, we can conclude that there is no relevant systematic error since all $|z_{score}|$ values resulted from using this function were less than 2.

It was also possible to prove that the self-absorption corrections provided by the Cutshall's model ($f_a^C$) does not work properly at low energies when selecting samples whose densities and <Z> are very high. Consequently, several methods were proposed in order to make the corrections provided by $f_a^C$ be valid. One of these proposed methods consisted of varying $h$, proving that as $h$ decreased, the $f_a^C$ validity increased. Regarding the other method, it consisted of placing the sample at different $d$ values (from 0 to 65 mm) and fixing $h$ at 25 mm. The $f_a^C$ validity increased as $d$ increased, which is very consistent since as $d$ increases, the parallelism requirements established by the Cutshall's model are fulfilled better. Finally, the same method employed to correct the TCS effects and make the $f_a^C$ validity be good, was used in order to correct the dead time, $t_d$. For this, three very active scales were chosen, achieving $t_d$ reductions up to 50%, which demonstrated the good validity of the proposed method.

### *CRediT authorship contribution statement*

**A. Barba-Lobo:** Conceptualization, Data curation, Formal analysis, Investigation, Methodology, Validation, Writing – original draft, Writing – review & editing. **J.P. Bolívar:** Conceptualization, Data curation, Formal analysis, Investigation, Methodology, Supervision, Validation, Writing – original draft, Writing – review & editing.

## Declaration of Competing Interest

The authors declare that they have no known competing financial interests or personal relationships that could have appeared to influence the work reported in this paper.

## Acknowledgments

This research has partially funded by the projects of the Regional Government of Andalusia called "Basic processes regulating the fractionations and enrichments of natural radionuclides under acid mine drainage conditions" (Ref.: UHU-1255876), and " Treatment of acid leachates from phosphogypsum piles located at Huelva, and transport modelling of the released radionuclides" (Ref.: P20_00096), the project funded by the Spanish Ministry of Science, Innovation and Universities' Research Agency "Development and optimization of a process for removing natural radionuclides in phosphogypsum leachates" (Ref.: PID2020-116461RB-C21), and the Project for Novel Principal Investigators " Quantitative study of the variables involved in the radon exhalation rate for granular solids; application to rafts of granular solid phosphogypsum " (Ref.: UHUPJ-00005-632) . The authors acknowledge the funding for open access charge provided by Universidad de Huelva / CBUA.

## Appendix A. Supplementary material

Supplementary data to this article can be found online at https://doi.org/10.1016/j.measurement.2022.111295.

## References

[1] G. Gilmore, J. Hemingway, Practical gamma-ray spectrometry, John Wiley & Sons, Chichester, 1995.
[2] A. Tedjani, C. Mavon, A. Belafrites, D. Degrelle, D. Boumala, D. Rius, J.E. Groetz, Well GeHP detector calibration for environmental measurements using reference materials, Nucl. Instrum. Methods Phys. Res. A 838 (2016) 12–17, https://doi.org/10.1016/j.nima.2016.09.022.
[3] Y. Venegas-Argumedo, M.E. Montero-Cabrera, True coincidence summing corrections for an extended energy range HPGe detector, AIP Conf. Proc. 1671 (2015), 030004, https://doi.org/10.1063/1.4927193.
[4] Z. Ahmed, In-Situ object calibration software (ISOCS) technique for $^{235}$U mass verification, Measurement 145 (2019) 648–650, https://doi.org/10.1016/j.measurement.2019.05.058.
[5] E.E. Belgin, G.A. Aycik, Derivation of an efficiency-calibration simulation for a well-type HPGe detector using the Monte Carlo approach and analytical techniques, Radiat. Meas. 73 (2015) 36–45, https://doi.org/10.1016/j.radmeas.2014.10.003.
[6] F. Bochud, C.J. Bailat, T. Buchillier, F. Byrde, E. Schmid, J.-P. Laedermann, Simple Monte-Carlo method to calibrate well-type HPGe detectors, Nucl. Instrum. Methods Phys. Res. A 569 (2006) 790–795, https://doi.org/10.1016/j.nima.2006.09.040.
[7] J.-M. Laborie, G.L. Petit, D. Abt, M. Girard, Monte Carlo calculation of the efficiency response of a low-background well-type HPGe detector, Nucl. Instrum. Methods Phys. Res. A 479 (2002) 618–630, https://doi.org/10.1016/S0168-9002(01)00942-1.
[8] N.L. Maidana, V.R. Vanin, J.A. García-Álvarez, M. Hermida-López, L. Brualla, Experimental HPGe coaxial detector response and efficiency compared to Monte Carlo simulations, Appl. Radiat. Isot. 108 (2016) 64–74, https://doi.org/10.1016/j.apradiso.2015.12.001.
[9] E. Sahiner, N. Meriç, A trapezoid approach for the experimental total-to-peak efficiency curve used in the determination of true coincidence summing correction factors in a HPGe detector, Radiat. Phys. Chem. 96 (2014) 50–55, https://doi.org/10.1016/j.radphyschem.2013.08.013.
[10] J.A. Suárez-Navarro, A.M. Moreno-Reyes, C. Gascó, M.M. Alonso, F. Puertas, Gamma spectrometry and LabSOCS-calculated efficiency in the radiological characterisation of quadrangular and cubic specimens of hardened portland cement paste, Radiat. Phys. Chem. 171 (2020), 108709, https://doi.org/10.1016/j.radphyschem.2020.108709.
[11] H. Zhu, R. Venkataraman, W. Mueller, J. Lamontagne, F. Bronson, K. Morris, A. Berlizov, X-ray true coincidence summing correction in Genie 2000, Appl. Radiat. Isot. 67 (2009) 696–700, https://doi.org/10.1016/j.apradiso.2009.01.013.
[12] J. Carrazana, N. Cornejo, M. Jurado, E. Capote, The effect of source chemical composition on the self-attenuation corrections for low-energy gamma-rays in soil samples, Appl. Radiat. Isot. 68 (2010) 360–363, https://doi.org/10.1016/j.apradiso.2009.10.013.
[13] E.G. San Miguel, J.P. Pérez-Moreno, J.P. Bolívar, R. García-Tenorio, J.E. Martin, $^{210}$Pb determination by gamma spectrometry in voluminal samples (cylindrical geometry), Nucl. Instrum. Methods Phys. Res. A 493 493 (1-2) (2002) 111–120.
[14] M. Xhixha-Kaçeli, New gamma-ray spectrometry methods for estimating K, U, Th concentrations in rocks of the Sardinia Batholith, Ph.D. Thesis (2013), University of Sassari, https://core.ac.uk/reader/19979790.
[15] A. Barba-Lobo, F. Mosqueda, J.P. Bolívar, A general function for determining mass attenuation coefficients to correct self-absorption effects in samples measured by gamma spectrometry, Radiat. Phys. Chem. 179 (2021), 109247, https://doi.org/10.1016/j.radphyschem.2020.109247.
[16] M. Bonczyk, Determination of $^{210}$Pb concentration in NORM waste – An application of the transmission method for self-attenuation corrections for gamma-ray spectrometry, Radiat. Phys. Chem. 148 (2018) 1–4, https://doi.org/10.1016/j.radphyschem.2018.02.011.
[17] M. Długosz-Lisiecka, M. Ziomek, Direct determination of radionuclides in building materials with self-absorption correction for the 63 and 186 keV γ-energy lines, J. Environ. Radioact. 150 (2015) 44–48, https://doi.org/10.1016/j.jenvrad.2015.07.018.
[18] IAEA, Preparation of gamma-ray spectrometry reference materials RGU-1, RGTh-1 and RGK-1. Report-IAEA/RL/148, Vienna (1987), https://nucleus.iaea.org/sites/ReferenceMaterials/Shared%20Documents/ReferenceMaterials/Radionuclides/IAEA-RGTh-1/rl_148.pdf.
[19] IAEA, Reference materials (2020), https://nucleus.iaea.org/sites/ReferenceMaterials/Pages/Index-for-Radionuclides.aspx.
[20] L. Barbero, M.J. Gázquez, J.P. Bolívar, M. Casas-Ruíz, A. Hierro, M. Baskaran, M. E. Ketterer, Mobility of Po and U-isotopes under acid mine drainage conditions: an

experimental approach with samples from Río Tinto area (SW Spain), J. Environ. Radioact. 138 (2014) 384–389, https://doi.org/10.1016/j.jenvrad.2013.11.004.
[21] M.J. Gázquez, J. Mantero, F. Mosqueda, J.P. Bolívar, R. García-Tenorio, Radioactive characterization of leachates and efflorescences in the neighbouring areas of a phosphogypsum disposal site as a preliminary step before its restoration, J. Environ. Radioact. 137 (2014) 79–87, https://doi.org/10.1016/j.jenvrad.2014.06.025.
[22] A. Hierro, M. Olías, C.R. Cánovas, J.E. Martín, J.P. Bolívar, Trace metal partitioning over a tidal cycle in an estuary affected by acid mine drainage (Tinto estuary, SW Spain), Sci. Total Environ. 497 (498) (2014) 18–28, https://doi.org/10.1016/j.scitotenv.2014.07.070.
[23] V. Spasic-Jokic, L. Zupunski, I. Zupunski, Measurement uncertainty estimation of health risk from exposure to natural radionuclides in soil, Measurement 46 (2013) 2376–2383, https://doi.org/10.1016/j.measurement.2013.04.019.
[24] A. Barba-Lobo, F. Mosqueda, J.P. Bolívar, An upgraded lab-based method to determine natural γ-ray emitters in NORM samples by using Ge detectors, Measurement 186 (2021), 110153, https://doi.org/10.1016/j.measurement.2021.110153.
[25] D. Grozdanov, I. Ruskov, N. Janeva, Y.N. Kopach, S.I. Negovelov, Y.D. Mareev, Determination of the dead-time losses in NaI(Tl) gamma-ray spectrometer, ISINN-21 proceedings (2015) 1-8, http://isinn.jinr.ru/proceedings/isinn-21/pdf/grozdanov.pdf.
[26] S.M. Karabidak, Dead Time in the Gamma-Ray Spectrometry, INTECH 2 (2017) 29-46, https://www.intechopen.com/books/new-insights-on-gamma-rays/dead-time-in-the-gamma-ray-spectrometry.
[27] G.F. Knoll, Radiation detection and measurement, Jhon Wiley and Sons, New York, 2000.
[28] S.G. Prussin, Prospects for near State-of-the art analysis of complex semiconductor spectra in the small laboratory, Nucl. Instr. Meth. 193 (1982) 121–128, https://doi.org/10.1016/0029-554X(82)90685-1.
[29] DDEP, 2017. The Decay Data Evaluation Project, http://www.nucleide.org/DDEP_WG/DDEPdata.htm.
[30] A.R. Agha, S.A. El-Mongy, A.E. Kandel, Assay of uranium isotopic ratios 234U/238U, 235U/238U in bottom sediment samples using destructive and non destructive techniques (Nasser Lake), Proceedings of the eighth Nuclear and Particle Physics Conference (NUPPAC-2011) 43 (2011) 221-229, https://inis.iaea.org/search/search.aspx?orig_q=RN:43099476.
[31] N.H. Cutshall, I.L. Larsen, C.R. Olsen, Direct analysis of $^{210}$Pb in sediment samples: Self-absorption corrections, Nucl. Instrum. Methods Phys. Res. A 206 (1983) 309–312, https://doi.org/10.1016/0167-5087(83)91273-5.
[32] K. Debertin, R.G. Helmer, Gamma- and X-ray spectrometry with semiconductor detectors, Elsevier, Amsterdam, 1988.
[33] P. Jodłowski, Self-absorption correction in gamma-ray spectrometry of environmental samples – an overview of methods and correction values obtained for the selected geometries, Nukleonika 51 (2006) 21-25, https://inis.iaea.org/search/searchsinglerecord.aspx?recordsFor=SingleRecord&RN=37115245.
[34] A. Barba-Lobo, E.G. San Miguel, R.L. Lozano, J.P. Bolívar, A general methodology to determine natural radionuclides by well-type HPGe detectors, Measurement 181 (2021) 109561.
[35] IND04-MetroMetal, Ionising radiation metrology for the metallurgical industry: Procedural guide for calculation of true coincidence summing correction factors for samples in metallurgical industry (2013), http://projects.ciemat.es/documents/16805/0/IND-04-12.pdf/e5d1682f-fbdb-42df-a0a3-9c573e8de3f2.
[36] P.R. Bevington, D. Keith, Data reduction and error analysis for the physical sciences, McGraw-Hill, New York (1969), https://www.scirp.org/(S(i43dyn45teexjx455qlt3d2q))/reference/ReferencesPapers.aspx?ReferenceID=1813409.
[37] P.G. Appleby, N. Richardson, P.J. Nolan, Self-absorption corrections for well-type germanium detectors, Nucl. Instrum. Methods Phys. Res. B 71 (1992) 228–233, https://doi.org/10.1016/0168-583X(92)95328-O.